Lasing on surface states in vertical-cavity surface-emission lasers

Yonan Su,[1] Chun-Yan Lin,[1] Ray-Ching Hong,[1] Wen-Xing Yang,[1,2] Chien-Chung Jeng,[3] Tien-Chang Lu,[4] and Ray-Kuang Lee[1,*]

[1]*Institute of Photonics Technologies, National Tsing-Hua University, Hsinchu 300, Taiwan*

[2]*Department of Physics, Southeast University, Nanjing 210096, China*

[3]*Department of Physics, National Chung-Hsing University, Taichung 402, Taiwan*

[4]*Department of Photonics, National Chiao Tung University, Hsinchu 300, Taiwan*

**Corresponding author: rklee@ee.nthu.edu.tw*

Received June 23, 2014; revised August 8, 2014; accepted August 10, 2014; posted August 13, 2014 (Doc. ID 214610); published September 22, 2014

We report experimental observation of lasing on surface states, in the form of standing waves at the termination of a defect-free photonic crystal on top of vertical-cavity surface-emission lasers. Direct images of lasing modes at the truncated periodic potential, along one side of a square lattice, are demonstrated by collecting near-field radiation patterns, as well as in numerical simulations. Our results provide a step toward realizing surface and edge states in optical cavities. © 2014 Optical Society of America

OCIS codes: (240.6690) Surface waves; (240.0240) Optics at surfaces; (140.7260) Vertical cavity surface emitting lasers; (140.3948) Microcavity devices.

http://dx.doi.org/10.1364/OL.39.005582

As a result of state-of-the-art semiconductor technologies, microcavities have served as a controllable platform to manipulate photons with small-mode volumes and ultrahigh qualify factors [1,2]. Through the correspondence between classical and quantum waves, studies on the lasing modes in vertical-cavity surface-emission lasers (VCSELs) demonstrate an alternative way to attack the fundamental issues and problems in quantum chaos and statistical mechanics [3–6]. In addition to the cavity modes supported with periodic orbits, standing waves can exist at the edge of a truncated lattice potential, known as the Tamm state [7]. As the electronic counterpart located at the interface separating periodic crystalline lattice and homogeneous vacuum space, optical surface states also exist at the termination of photonic crystal (PhC) or periodic waveguide arrays [8,9]. However, to remain localized states inside the "light core" defined by the free-space dispersion relation, optical Tamm states appear at the interface of two PhCs [10,11]. With the introduction of metallic structures, strongly confined plasmonic surface modes are revealed at the interface of metal-dielectric metamaterials [12–14], as the electronic Shockley state does in the metal-lattice structure [15]. Moreover, surface solitons can be induced through optical nonlinearities [16,17], which extend the concept of surface states from one-dimensional (1D) lines to two-dimensional (2D) ring configurations [18,19]. A variety of optical devices based on the surface waves have been demonstrated, with potential applications in optical filters, sensors, switchers, and absorbers.

To create optical surface states, truncated planar multilayer or PhC structure are used with normal incident light [20,21]. With a large transverse lasing area compared to the cavity length, in this Letter, we fabricate a 2D square lattice on top of a VCSEL to study optical surface states in mesoscopic systems. Without introducing any defect modes, we report experimental observation of lasing patterns as optical surface states by directly collecting their near-field radiation intensities at room temperature. Even in the absence of metallic materials, the measured optical surface states have the main peak in their intensity profiles located outside the PhC layer, since our surface microstructure has a lower refractive index. As the first observation on the electronic Tamm states, our defect-free PhC acts as a superlattice [22]. Direct numerical simulations based on a 2D mode solver verify our experimental measurement. With recent demonstration of optical edge states as topological insulators [23], the results shown in our experimental observations and simulations provide an alternative but effective approach to access surface modes in electrical-pumped VCSELs.

Our device is fabricated on an ion-implanted VCSEL, with the schematic diagram shown in Fig. 1(a). The epitaxial layers of VCSELs are grown by metal organic chemical vapor deposition (MOCVD) on a n^+-GaAs substrate, with a graded-index separate confinement heterostructure (GRINSCH) active region formed by undoped triple-GaAs-AlGaAs multiple quantum wells (MQW) placed in one lambda cavity. The emitting aperture is confined by the p metal in the square configuration, with the length of $D_2 = 60$ μm; while the n contact is formed at the bottom of the n-GaAs substrate. The upper and bottom distributed Bragg reflectors (DBRs) in the vertical cavity consist of 22 and 35.5 pairs of $Al_{0:1}Ga_{0:9}As/Al_{0:9}Ga_{0:1}As$ layers, respectively. Then, reactive-ion etch (RIE) is performed to define mesas, by selectively oxidation to AlO_x. The thickness of the oxide layer is about 300 Å (within a quarter-λ layer, and $\lambda = 850$ nm). Detailed device parameters and lasing characteristics can be found in our previous work on similar VCSEL devices but with different surface microstructures [6,24]. On the surface, we etch the emitting window by the focus-ion beam (FIB) to 1 μm in depth, where a PhC structure in the square lattice is patterned. Here, the square lattice has the length $D_1 = 40$ μm, the lattice constant $R = 5$ μm, and the diameter of circles $d = 2$ μm, respectively, as shown in Fig. 1(b).

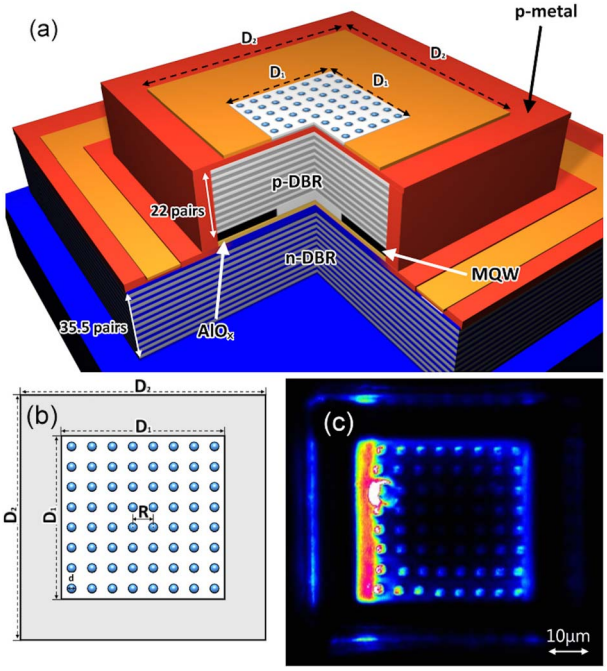

Fig. 1. (a) Schematic diagram of the device structure. On top of the surface is a defect-free photonic crystal structure depicted in (b). The surface structure is designed with the length $D_1 = 40$ μm and $D_2 = 60$ μm for the inner and outer squares; while the square lattice has a lattice constant $R = 5$ μm and diameter of circles $d = 2$ μm, respectively. (c) One example of optical surface states is observed by the near-field intensity distributions on the surface of aperture, shown in false color, with the injection current $I = 30$ mA.

From the L–I curve, the light versus current, of this surface-structured VCSEL shown in Fig. 2, it is hard to see a clear threshold value of the injection current for the lasing condition. However, the slope of the L–I curve changes around the current of 30 mA, from 0.011 to 0.062 mW/mA. We measure the near-field electromagnetic intensity distribution at a fixed injection current by a charge-coupled device (CCD) camera through a standard microscope with a 100× lens. The emission

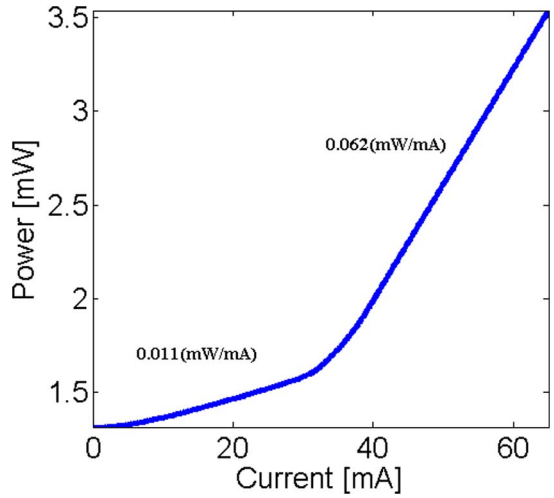

Fig. 2. L–I curve, power versus current for our VCSEL. One can see that the curve changes its slope around the current at 30 mA, from 0.011 to 0.062 mW/mA.

pattern at the injection current of 30 mA is shown in Fig. 1(c), which reveals the lasing mode at the interface between the patterned square lattice in the center and the homogeneous background around it. A bright spot, which we believe should come from the imperfect fabrication process, is also observed. Nevertheless, the radiation field reflects the geometric structure of our patterned square lattice. It can be seen clear that only one side of the square shows a strong radiation intensity in the shape of a line.

By increasing the injection current, in Fig. 3, we show a series of the measured near-field images at the currents of 42.8, 57.3, 58, and 65 mA, respectively. All of these radiation patterns share a common feature, that is, lasing along the termination of periodic potentials. With the enlarged images, the intensity distribution is not a constant along the edge, denoted as the y axis here, but with a sinusoidal profile according to the index modulation. By taking the cross-section of intensity profiles in the horizontal direction, denoted as the x axis along the dashed lines depicted in Figs. 3(a)–3(d), we plot the intensity distributions of these optical surface states in Figs. 3(i)–3(l), respectively. To have a clear illustration, we also show the corresponding refractive-index modulation in the shadowed region. In Fig. 3(i), one can see that the observed optical surface state has the main peak in the profile located at the interface, or more exactly outside the periodic potential, due to a higher refractive index there. Moreover, this optical surface state possesses a long oscillatory tail inside the lattice potential, which demonstrates the manifold of periodic Bloch waves. Due to the modulation of the refractive index, the oscillation peaks occur at the valleys of the lattice potentials. Compared to the known reports in the literature with dielectric modulations to support surface states, our optical surface states reside outside the lattice potential, which behaves more like those surface states confined by the metallic media. However, from Figs. 3(i)–3(l), the location of the main peak in the profile for these optical surface states remains almost unchanged for different injection currents; while the strength in the oscillatory tail varies strongly.

To further understand our experimental observation of lasing on optical surface states in such a surface microstructured VCSEL, we use a 2D mode solver based on the standard finite-element method for electromagnetic waves (COMSOL Multiphysics) to calculate the corresponding eigenmodes [24]. Here, we reduce the original three-dimensional (3D) configuration into an effective 2D model by estimating the effective index, due to the optical field being confined by two DBR mirrors, with the oxide layer of thickness about 300 Å in the vertical direction. The lateral geometry is defined by the diagram shown in Fig. 1(b). The effective refractive indices are assumed to be 1 in the holes and 3.49 in the surrounding oxide layer. Dirichlet boundary conditions are applied for the surrounding p metal. In the numerical simulations, we calculate all possible eigenmodes and then select the ones that match the most as the possible optical surface states, for the reason that these found eigenmodes are nearly degenerate, with very close eigenwavelengths around the lasing wavelength at 850 nm. As a comparison, the selected numerical eigenmodes are shown in

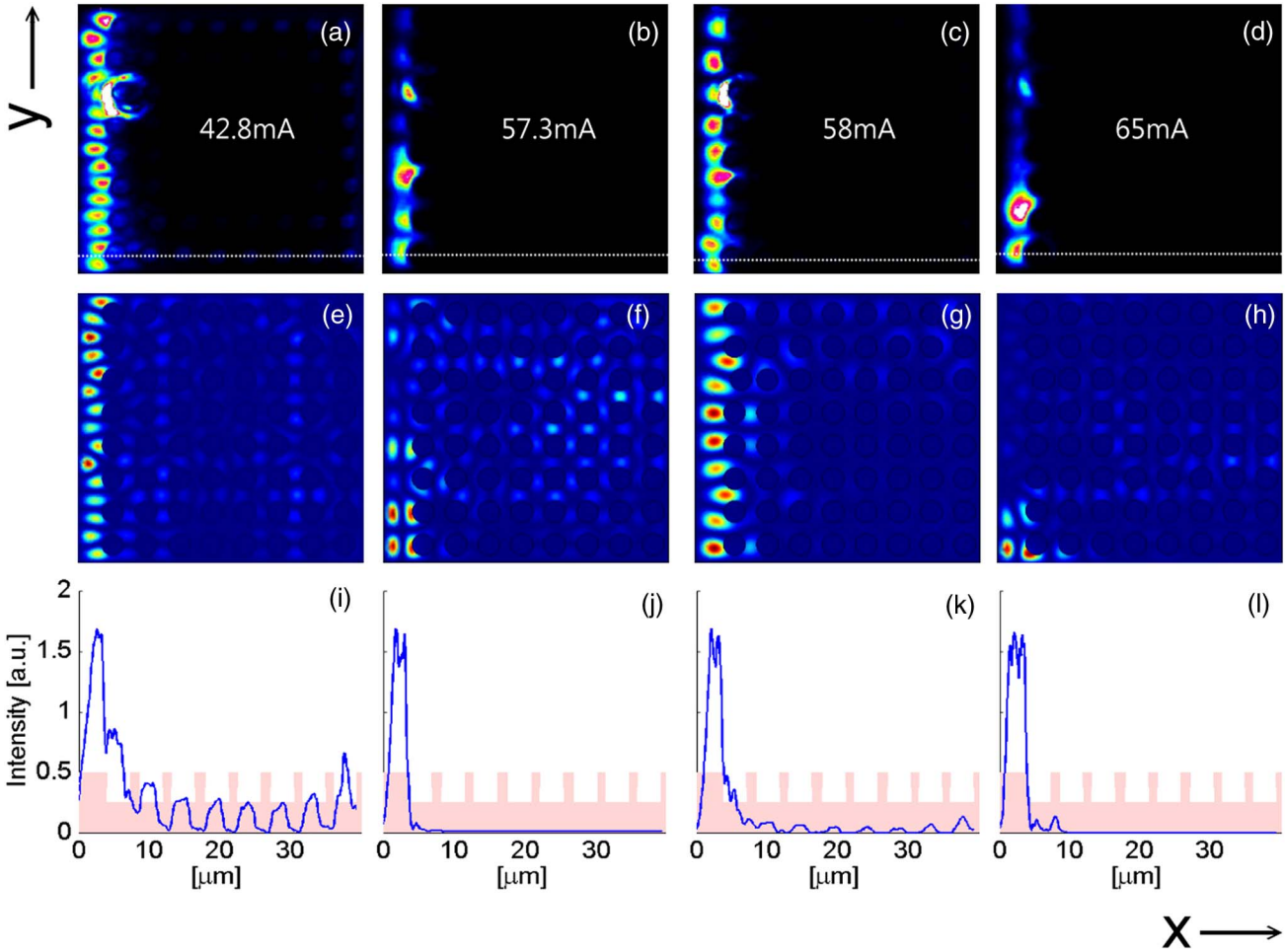

Fig. 3. Experimental near-field images of lasing modes are measured at the injection currents (a) 42.8 mA, (b) 57.3 mA, (c) 58 mA, and (d) 65 mA, respectively. (e)–(h) show the corresponding eigenmodes selected from directly numerical simulations. The cross-sections of the intensity profiles along the dashed lines shown in (a)–(d) are depicted in (i)–(l) in solid curves, while the shadow regions shown are the corresponding profiles of refractive-index modulation.

Figs. 3(e)–3(h), which give good agreement to our experimental measurements in Figs. 3(a)–3(d). Moreover, we note that the observed optical surface states can appear on every side of the square in numerical simulations; while in experiments lasing modes are found only on a particular side. Some unwanted imperfection accounts for the latter.

In summary, with a large transverse lasing area, we fabricated a defect-free square lattice on top of a VCSEL and reported experimental observation of lasing on optical surface states at the termination of lattice potential. Unlike the optical surface states supported inside the waveguide array, our localized lasing states are located outside the truncated photonic lattice. By varying the injection currents, the main peak in the intensity profile of these observed optical surface states remains almost unchanged. With these experimental observations and simulation results, applications based on optical surface modes in semiconductor lasers are expected.

The authors are indebted to Dr. T.-D. Lee for providing the samples. This work is partly supported by the Ministry of Science and Technology, Taiwan. The research is also supported in part by National Natural Science Foundation of China under Grant No. 11374050, by Qing Lan project of Jiangsu, and by the Fundamental Research Funds for the Central Universities under Grant No. 2242012R30011.

References

1. R. K. Chang and A. J. Campillo, eds., *Optical Processes in Microcavities* (World Scientific, 1996).
2. K. J. Vahala, ed., *Optical Microcavities* (World Scientific, 2004).
3. J. U. Nockel and A. D. Stone, Nature **385**, 45 (1997).
4. C. Gmachl, F. Capasso, E. E. Narimanov, J. U. Nockel, A. D. Stone, J. Faist, D. L. Sivco, and A. Y. Cho, Science **280**, 1556 (1998).
5. T.-D. Lee, C.-Y. Chen, Y. Y. Lin, M.-C. Chou, T.-H. Wu, and R.-K. Lee, Phys. Rev. Lett. **101**, 084101 (2008).
6. Y. Y. Lin, C.-Y. Chen, W. Chein, J. S. Pan, T.-D. Lee, and R.-K. Lee, Appl. Phys. Lett. **94**, 221112 (2009).
7. I. E. Tamm, Z. Phys. **76**, 849 (1932).
8. P. Yeh, A. Yariv, and A. Y. Cho, Appl. Phys. Lett. **32**, 104 (1978).
9. A. Szameit, I. L. Garanovich, M. Heinrich, A. A. Sukhorukov, F. Dreisow, T. Pertsch, S. Nolte, A. Tünnermann, and Yu. S. Kivshar, Phys. Rev. Lett. **101**, 203902 (2008).
10. J. D. Joannopoulos, R. D. Meade, and J. N. Winn, *Photonic Crystals*, 2nd ed. (Princeton University, 2008).
11. A. V. Kavokin, I. A. Shelykh, and G. Malpuech, Phys. Rev. B **72**, 233102 (2005).

12. S. M. Vukovic, I. V. Shadrivov, and Yu. S. Kivshar, Appl. Phys. Lett. **95**, 041902 (2009).
13. S. H. Nam, E. Ulin-Avila, G. Bartal, and X. Zhang, Opt. Lett. **35**, 1847 (2010).
14. Y. Y. Lin, R.-K. Lee, and Yu. S. Kivshar, Opt. Lett. **34**, 2982 (2009).
15. W. Shockley, Phys. Rev. **56**, 317 (1939).
16. S. Suntsov, K. G. Makris, D. N. Christodoulides, G. I. Stegeman, A. Haché, R. Morandotti, H. Yang, G. Salamo, and M. Sorel, Phys. Rev. Lett. **96**, 063901 (2006).
17. X. Wang, A. Bezryadina, and Z. Chen, Phys. Rev. Lett. **98**, 0123903 (2007).
18. C. P. Jisha, Y. Y. Lin, T.-D. Lee, and R.-K. Lee, Phys. Rev. Lett. **107**, 183902 (2011).
19. K.-H. Kuo, Y. Y. Lin, and R.-K. Lee, Opt. Lett. **38**, 1077 (2013).
20. A. P. Vinogradov, A. V. Dorofeenko, S. G. Erokhin, M. Inoue, A. A. Lisyansky, A. M. Merzlikin, and A. B. Granovsky, Phys. Rev. B **74**, 045128 (2006).
21. A. Kavokin, I. Shelykh, and G. Malpuech, Appl. Phys. Lett. **87**, 261105 (2005).
22. H. Ohno, E. E. Mendez, J. A. Brum, J. M. Hong, F. Agullo-Rueda, L. L. Chang, and L. Esaki, Phys. Rev. Lett. **64**, 2555 (1990).
23. Z. Wang, Y. Chong, J. D. Joannopoulos, and M. Soljacić, Nature **461**, 772 (2009).
24. C. J. Cheng, Y. Y. Lin, C.-Y. Chen, T.-D. Lee, and R.-K. Lee, Appl. Phys. B **97**, 619 (2009).